Sensors and Actuators A 242 (2016) 9–17

Contents lists available at ScienceDirect

Sensors and Actuators A: Physical

journal homepage: www.elsevier.com/locate/sna

Micro catalytic methane sensors based on 3D quartz structures with cone-shaped cavities etched by high-resolution abrasive sand blasting

Wenshuai Lu [a], Gaoshan Jing [a], Xiaomeng Bian [a], Hongyan Yu [a], Tianhong Cui [b,*]

[a] State Key Laboratory of Precision Measurement Technology and Instruments, Department of Precision Instruments, Tsinghua University, Beijing, 100084, China

[b] Department of Mechanical Engineering, University of Minnesota, Minneapolis, MN 55455, USA

ARTICLE INFO

Article history:
Received 17 November 2015
Received in revised form 2 February 2016
Accepted 6 February 2016
Available online 11 February 2016

Keywords:
Methane sensor
MEMS
Quartz
Abrasive sand blasting

ABSTRACT

A novel quartz based micro catalytic methane sensor with back-etched cone-shaped cavity was fabricated by high-resolution abrasive sand blasting technique. Highly uniform micro cavities were easily and quickly achieved with a depth of 450 μm and a bottom diameter of 600 μm on a quartz substrate 500 μm thick, followed by screen printing porous alumina with a position accuracy of 10 μm and inkjet printing of co-metal catalyst with loading quantity resolution of 4.75 ng. Compared with a bulk quartz substrate sensor, performance of the sensor fabricated by abrasive sand blasting is greatly improved with a lower thermal mass. The sensor's temperature distribution profile is more concentrated on target catalyst, power consumption decreases to 285 mW by 23%, thermal response time decreases to 8.8 s by 79%, and sensitivity to methane increases to 1.83 mV/% CH_4 by 35%, with a high correlation coefficient up to 0.9986. Moreover, this sensor demonstrates excellent resistance to mechanical shock at high working temperatures, significantly superior to conventional silicon based membrane sensors. This design of the high performance sensor, together with the simple and fast MEMS-compatible fabrication process enables such catalytic sensors for mass production and combustible gas detecting in harsh environmental applications.

1. Introduction

Methane is a common and important alkane gas for both industrial applications and civilization life, including great uses for energy supply and chemical industry. However, methane leakage makes significant threats to human life and the environment due to its combustible and greenhouse properties. On one hand, methane is highly explosive in air atmosphere within the volume fraction ranging from 5% to 15% (so called "explosive limits"), resulting in casualties in coal mining or natural gas exploration [1–3]. On the other hand, the greenhouse effect of methane is 20 times of carbon dioxide, which cannot be neglected for natural gas pipeline or vehicle exhausts [4,5]. Therefore, sensitive methane detection attracts more and more attentions of the public, especially for portable or wearable methane sensing [6]. Among the main techniques of combustible gas sensors including catalytic combustion sensor, metal-oxide semiconductor sensor, infrared absorption sensor, and thermal conductivity sensor, catalytic combustion sensor accounts for the most market share [7] due to its simple structure, miniature size, low cost, and high stability [8,9]. A traditional coil-bead catalytic gas sensor (pellister) consists of a platinum coil resistor covered by alumina with noble metal catalyst. The coil resistor provides a proper initial working temperature from 400 °C to 500 °C as a heater for the catalyst, and senses the reaction heat released by catalytic combustion of methane with oxygen at the same time, which raises the temperature of the resistor inducing a resistance increase [10]. Ideally, the increase of the resistance is proportional to the concentration of methane below the lower explosive limit of methane (5%) [11]. Although catalytic sensors are widely utilized in coal mining, the relative high power consumption and the manual fabrication process impede further applications of this type of sensors [12], for example the Internet of Things (IoT), with needs for extremely low power, chip-level size, and automatic mass production [7,13].

Methane gas sensors based on silicon hotplate solves the above problems, with the advantages of automatic micromachining processes and miniature thermal dissipation decreasing the heating power [14,15]. However, there are new problems for the conventional silicon membrane limiting the applications of MEMS catalytic sensor. On one hand, the thermal conductivity of silicon is as high

* Corresponding author.
E-mail addresses: tcui@me.umn.edu, cuixx006@umn.edu (T. Cui).

http://dx.doi.org/10.1016/j.sna.2016.02.017
0924-4247/

as 149 W/m K, inducing large thermal loss unless a suspended membrane structure is fabricated. However, the fabrication of this membrane structure is complex with a series of processes including thermal oxidation, chemical vapor deposition, reactive ion etching, and wet etching, resulting in a low yield [16,17]. On the other hand, the membrane (mostly Si_3N_4 or SiO_2) together with heating electrodes (mostly platinum) is usually less than 1 μm thick [18,19], which is fragile and not compatible with contact loading fabrication of porous catalyst [20], such as screen printing. Moreover, due to the suspended membrane beams with low strength and the catalyst layer much thicker than the membrane [21], the membrane sensor can hardly resist mechanical shock at high working temperatures, inducing a permanent strain to the membrane together with the platinum electrode, and thus generate a bias to the output signal [22], or even cause a crack of the structures [23,24]. To solve the manufacturing and structural problems of silicon based membranes, in our previous work we have proposed and demonstrated bulk fused quartz as a low power substrate for micro catalytic methane sensor without a membrane structure due to its low thermal conductivity (1.2 W/m K) based on simple microfabrication processes, demonstrating reliable performance and good compatibility with high-resolution screen printing of porous alumina [25].

In this paper, to further enhance the sensor performance by reducing the thermal mass of the heating and sensing region, a new 3D quartz structure for micro catalytic methane sensors with a back etched cone cavity was proposed and verified by finite element modelling (FEM) simulation, and uniformly fabricated by high-resolution abrasive sand blasting with an etching rate of 380 μm/s. By adjusting the effective sand blasting time to 1169 ms on a single cavity, 450 μm thick cone cavities on a quartz substrate 500 μm thick were simply and uniformly achieved, with bottom diameter of 600 μm, inclination angle of 20°, and surface roughness of 1 μm. The proposed structure demonstrates good compatibility with screen printing and inkjet printing, by which high-quality alumina with bimetallic catalyst was deposited on the front surface of sensors [26]. Compared with bulk quartz sensors, the performance of the cone-shaped sensor improves significantly, with a power consumption to 285 mW decreased by 23%, thermal response time to 8.8 s reduced by 79%, sensitivity to 1.83 mV/vol.% CH_4 increased by 35%, and linear coefficient increased from 0.9856 to 0.9986. In addition, compared with silicon based membrane sensors, the fabricated cone-shaped quartz sensor demonstrates a high resistance to external mechanical vibration at 450 °C, while the silicon based membrane sensors show notable fluctuation influenced by vibrations reported by other groups [27,28].

This sensor design together with the cone-shaped quartz micro hotplate and the integrated MEMS compatible processes, including abrasive sand blasting, screen printing, and inkjet printing, provides a universal platform for fabrications of micro catalytic combustion device and shows good prospect in harsh environmental applications.

2. Materials and methods

2.1. Model design and FEM simulation

The cone-shaped quartz micro hotplate for a catalytic sensor was designed and simulated by COMSOL Multiphysics software (COMSOL Inc., USA). The FEM model of the micro hotplate is shown in Fig. 1a. A platinum electrode 400 nm thick as both a heater and a temperature sensor was designed on a quartz substrate 500 μm thick. The heating area of the electrode is designed as a rectangular pattern 260 μm by 50 μm rather than a square wave pattern to simplify the meshing of the simulation. Two gold circular patterns were embedded in both sides of the platinum electrode as gold ball bonding pads, with diameter of 25 μm and center distance of 400 μm. A cone-shaped cavity with bottom diameter of 600 μm and inclination angle of 20° was back caverned beneath the heating area. The thickness of the cavity was varied from 10 μm to 475 μm as a variable parameter. The substrate was fixed to a semi-infinite thermal bulk by thermal resist glue [29]. Thermal physics module of *Heat Transfer in Solid* was utilized to the whole model, which was surrounded by air and free convective flux enabled, with a heat transfer coefficient of 5 W/(m^2 K) as the boundary condition, a typical value for natural convection heat transfer between thermal device and ambient air [30,31]. None domain was set as thermal insulation. Electrical physics module of *Electric Current* was utilized to the electrode and the bonding pads, with one point set to a tunable input voltage, and another to the ground. The electrode was set as high thermal conductivity layer, while the resistive heat loss in the circuit was defined as heat source by enabling electromagnetic heat. Multiphysics module of *Electromagnetic Heat Source* was utilized as the coupling of thermal and electrical modules. The electrode and cavity parts were meshed by free tetrahedral elements ranging from 2.24 to 7.68 μm, while the other parts were meshed by free triangular elements ranging from 152 to 3540 μm for fast simulation. The target average temperature of the heating area was set to 450 °C by tuning the driving voltage to a proper potential value, while the effects of the cavity depth on the sensor's power consumption and 90% response time were investigated as a guideline for the following device fabrication. The simulation results are shown in Fig. 1b, c and d.

From the 3D temperature distribution profile in transparency view as shown in Fig. 1b, the high temperature region (above 350 °C by yellow and red colors) concentrates on the surface of the target heating area on both x-y plane and z axis, demonstrating a high heating efficient. As shown in Fig. 1c and 1d, the cavity depth makes significant influences to the power consumption and the response time of the senor model. The power consumption decreases from 575 mW to 385 mW by 33% as the cavity's depth increases from 10 μm to 475 μm, while the response time decreases from 60 s to 8s by 87%. Finally, considering the possible yield of the sensors, 450 μm was selected as an optimized depth, with power consumption and response time decrease by 28% and 79%, respectively, given to the FEM simulation.

2.2. Device fabrication

The sensor fabrication processes together with its schematic diagram were designed, as shown in Fig. 2a to 2e. First, a 4-inch fused quartz wafer 500 μm thick was physically back-etched with alumina sand powder and soft mask by high-resolution abrasive sand blaster (WP SB002, WaferPlus, Taipei) at continuous scanning mode, with a horizontal moving speed of 3 m/min and an average etching rate over 380 μm/s. The mean particle size of the blasting alumina powder is 25 μm. Cone-shaped cavities were physical etched with bottom diameter of 600 μm and inclination angle of 20°, as shown in Fig. 2f. To verify the optimized depth of the cavity, various depths of 380 μm, 430 μm and 450 μm were fabricated with effective etching time of 847 ms, 1081 ms, and 1169 ms, respectively. The laboratory yield of these three depths cavities during sand blasting turned out to be 100%, 99%, and 96% out of three wafers including 924 units, while sand blasting over-etching will generate perforations through the quartz substrates. Meanwhile, a bulk quartz substrate 500 μm thick without abrasive blasting was also utilized to fabricate sensors as comparison. Second, electrode of 50 nm thick Ti and 400 nm thick Pt was patterned by the standard lift-off process. The details of the fabrication parameters are the same as our previous work [25]. As shown in Fig. 2g, the fabricated heating electrode is designed as a square wave pattern

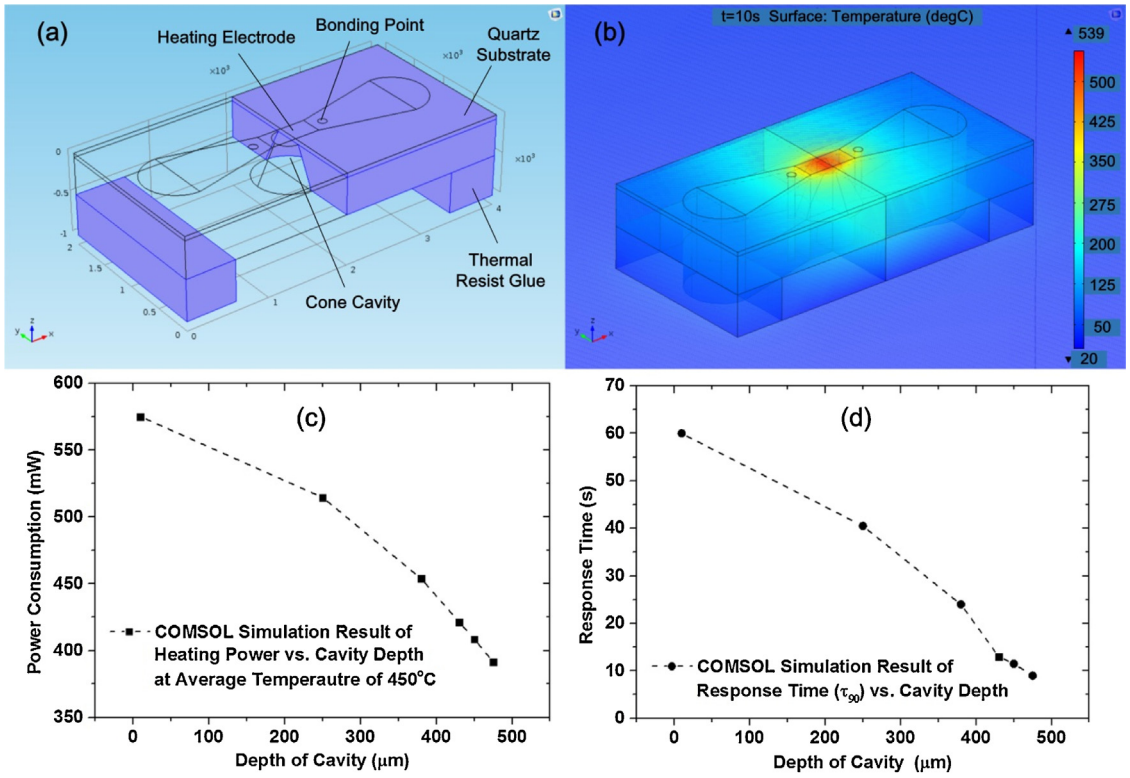

Fig. 1. FEM design and simulation results of the proposed 3D structure quartz sensor with back-etched cone-shaped cavity by COMSOL Multiphysics. (a) FEM model of the cone-shaped structure. (b) Simulation result (transparency view) of 3D temperature distribution profile at average working temperature of 450 °C, with high temperature concentrates on the surface of the target heating region. Simulation curves of (c) power consumption and (d) response time versus the depth of the cavity.

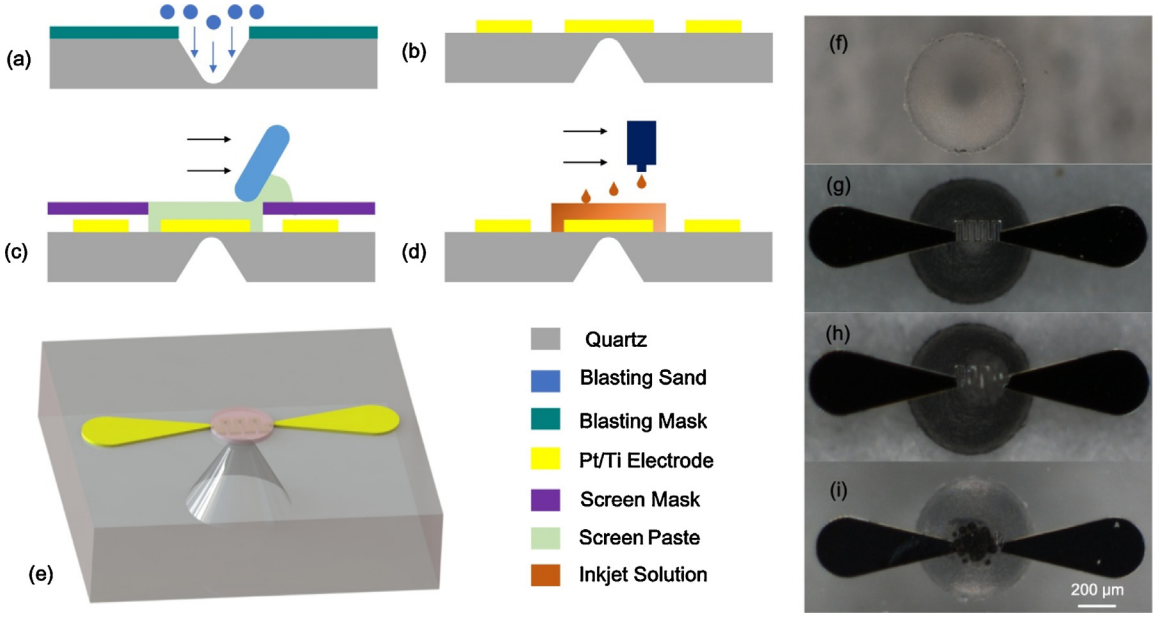

Fig. 2. Micro fabrication process of the proposed gas sensor including (a) abrasive sand blasting of the cone-shaped micro cavity with bottom diameter of 600 μm, (b) lift-off of the 50 nm thick Ti/400 nm thick Pt electrode, (c) screen printing of the alumina paste to pattern 10 μm thick porous support layer, (d) inkjet printing of the H_2PtCl_6 and $PdCl_2$ solutions to deposit bi-metal catalyst. (e) The schematic diagram of the proposed sensor based on the processes above. (f)–(i) Optical images of the fabricated device after every process corresponding to (a)–(d) respectively.

to increase the resistance to 80.0 Ω of the micro heater, to eliminate the contacting error induced by gold ball bonding (about 1.5 Ω) in the packaging process. Although the electrode patterns of the fabricated device and the FEM model are different, they cover the same heating area 260 μm by 50 μm, demonstrating similar relation between the power consumption and the working temperature. Third, a circular pattern of alumina paste (Senlont Electronic, China) with diameter of 300 μm was deposited by high-resolution screen printer (MT650, Micro-tec, Japan), followed by a calcining treatment in 550 °C for 2 h to form a layer of porous γ-Al_2O_3 support 10 μm thick, as shown in Fig. 2h. Last, appropriate quantities of micro droplets of H_2PtCl_6 (8 wt.% aqueous solution,

Sigma-Aldrich, USA) and $PdCl_2$ (5 wt.% in 10 wt.% hydrochloric acid solution, Sigma-Aldrich) were uniformly deposited onto the patterned porous alumina by inkjet printing to form 7Pd-3Pt catalyst, with an optimized loading resolution of 4.75 ng and a total loading mass of 10 wt.%, followed by 10 min of vacuum assisted impregnation and 2 h of calcining at 450 °C. The bimetallic catalyst was utilized for its combination of catalytic activity and stability [32,33], which is investigated by our previous work [26]. The accumulated alignment mismatch of the above processes was calculated as ±17.5 μm, with mismatches of ±7.5 μm, ±5 μm, and ±5 μm during sand blasting, screen printing, and inkjet printing respectively. Finally, the whole wafer was cut into 308 elements (2 mm by 2 mm) by a dicing saw (DAD-321, Disco, Japan), and a micro catalytic sensing element with cone-shaped cavity and porous alumina supported bimetallic catalyst was formed, as shown in Fig. 2i .

The fabricated gas sensing elements were then packaged into SOP8 sockets (Sunny Technologies, China) by gold ball bonding and thermal resist glue (HR8812, Huirui Adhesive, China) to form gas sensors, and were integrated into a constant current bridge circuit for measurement.

2.3. Structural, thermal, electrical and surface characterization

The profile of the blasted micro cavity was verified by optical microscopy. The morphologies of the cavity together with inner sidewall and inner bottom was characterized by scanning electron microscope (SEM, FEI Quanta 200, Oregon, USA). The depth of the cavities with different parameters was measured by white light interferometer (WLI, Coutour GT K1, Bruker, Germany), with the interference fringes focused on bottom and top of the cavity, respectively.

The distribution of the sensor temperature powered by tunable voltage was measured by a high resolution infrared camera (VarioCAM HD 880, InfraTec, Germany) with temperature accuracy of ±1.5 °C. The average working temperature of the heating area (5 by 3 pixels) is calculated by infrared image analyzing software (IRBIS3, InfraTec, Germany). 2D infrared images were compared between the blasted sensor and the bulk sensor working at 450 °C. Furthermore, surface temperature profiles distributed along the central line across the catalyst were analyzed, to further verify the heating efficient enhanced by the blasted cavity.

Relation between power consumption and working temperature was investigated among the sensors with different depth of cavities, while the response time affected by the depth was also analyzed by measuring the transient resistance during the powering procedure. The power consumption and the transient resistance were both calculated from the driving voltage and the response current, monitored by the data acquisition system (34972A, Keysight Technologies, USA).

Morphologies of the blasted sensor and the fresh alumina supported bimetallic catalyst were characterized by SEM, to validate the uniformity and porosity of the printed catalyst. The catalyst morphology after six hours aging treatment in 0.6% methane [34] with compressed air as carrier gas was also investigated by SEM as comparison to characterize the thermal stability of the fabricated bimetallic catalyst.

2.4. Sensing performance characterization

The integrated sensor with cavity structure 450 μm deep was fitted into a homemade glass chamber (15 L) with a gas delivering system and an infrared gas monitor (Ultramat-23, SIEMENS, Germany). Sensing performance to methane gas with concentration varied from 0.5% to 2.5% with compressed air was measured at working temperature of 450 °C. The sensor response signal was recorded by computer based automatic measuring system. Sensitivity and linear correlation coefficient were utilized to characterize the sensors performance. As a comparison, the bulk substrate sensor without a cavity was also measured. Additionally, the sensor's performance at elevated ambient temperatures was investigated by comparing base-line signals of the sensor's sensing element (with catalyst), reference element (without catalyst), and bridge (consist of a sensing/reference pair), with the sensor heated in an oven (GZX-9140 MBE, Boxun, China) with temperature changing from 20 °C to 50 °C.

The sensor resistance to mechanical shock at high temperatures was investigated together with a silicon based membrane gas sensor (MP7214, SGX Sensortech, UK) and a coil-bead gas sensor (MJC4-3.0, Winsen Electronics, China). These three sensors were soldered on the same PCB board fixed on a vibrator (MX-S, Dragon Lab, China) with vibrating amplitude of 4 mm and frequency of 50 Hz, and were powered and measured by the same electrical cables. The raw data of transient output signals during the vibration was recorded by Lab Windows/CVI program and was analyzed by OriginLab software.

3. Results and discussion

3.1. Structural, thermal, electrical and material properties

The optical image of the blasted micro cavity in quartz substrate is shown in Fig. 3a, demonstrating a uniform circular pattern with a sharp margin on the bottom of the cavity. The SEM images of the cavity's profile, margin, and inner surface are shown in Fig. 3b, 3c and 3d. In Fig. 3b, a cone-shaped structure with a dome-shaped top can be deduced by brightness, with the bottom and the top diameters of about 600 μm and 200 μm, respectively. The inclination angle of the cone is calculated to be about 23°. In Fig. 3c and d, a maximum margin crack of 10 μm and a sidewall roughness of 1 μm are achieved, while a uniform cone bottom with roughness less than 2 μm was achieved as shown in Fig. 3e and 3f, which demonstrated good compatibility of sand blasting process with a quartz substrate for back cavity fabrication.

The depth of the micro cavities was characterized, as shown in Fig. 4. By focusing the WLI on bottom (Fig. 4a) and top (Fig. 4b) of the cavities, the depth of the cavities designed as 380 μm, 430 μm, and 450 μm are measured to be 372.5 μm, 431.0 μm, and 455.5 μm, respectively, within a relative error of less than 2%.

The temperature distributing profiles of the blasted sensor and the bulk sensor with average temperature of 450 °C are shown in Fig. 5a and b, respectively. Just as the simulation result in Fig. 1b, the high temperature area of the blasted sensor (above 250 °C colored by green in the infrared image) is more concentrated on the surface of the target catalyst, while the high temperature area of the bulk sensor is about twice of the former one. From Fig. 5c, the enhancement of heating efficient can be further confirmed. The temperature on edge of the blasted sensor chip is just 120 °C, while it is 200 °C on the bulk chip, showing a larger waste of heating power.

The sensor's steady state thermal response was investigated by comparison of the power consumption versus the working temperature (average temperature with 5 by 3 pixels) as shown in Fig. 6. When the cavity depth increases from 0 to 450 μm, the heating power decreases monotonically from 370 mW to 285 mW by 23%, indicating that a lower thermal mass induces a lower heat loss. Meanwhile, the sensor's transient thermal response was investigated by comparing the thermal response time (τ_{90}) versus different depth of cavities as shown in Fig. 7, with the response curves plotted from recorded normalized resistance. As the depth increases from 0 to 450 μm, the 90% response time shortens monotonically from 42.0 s to 8.8 s by 79%, which demonstrates that a

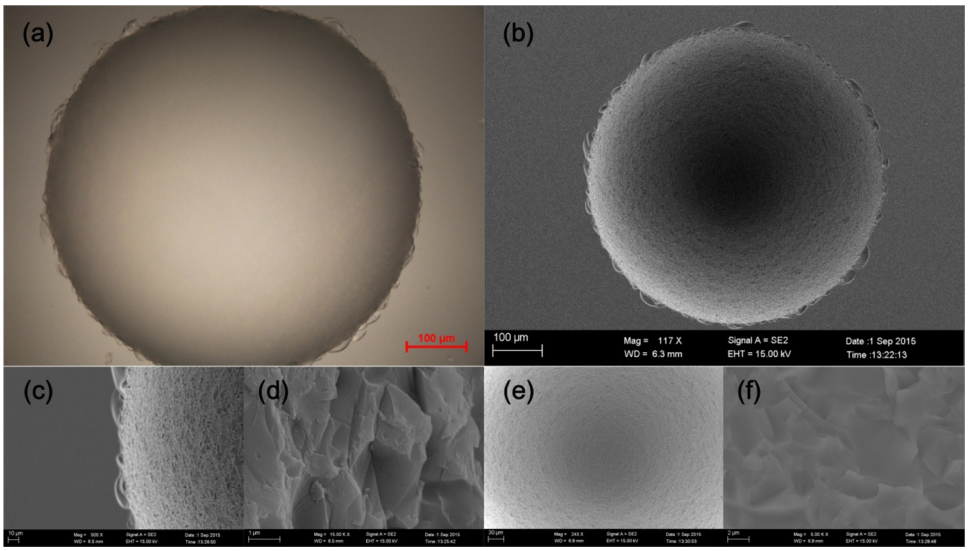

Fig. 3. Structural characterization results of the micro cavity. (a) Optical profile of the micro cavity with a sharp circular margin. (b) SEM image with gradual change of brightness, from which a cone-shaped structure can be deduced. (c) SEM image of the cavity's margin with crack less than 10 μm. (d) SEM image of cavity's inner sidewall with roughness of 1 μm. (e) to (f) SEM images of cavity inner bottom surface with roughness less than 2 μm.

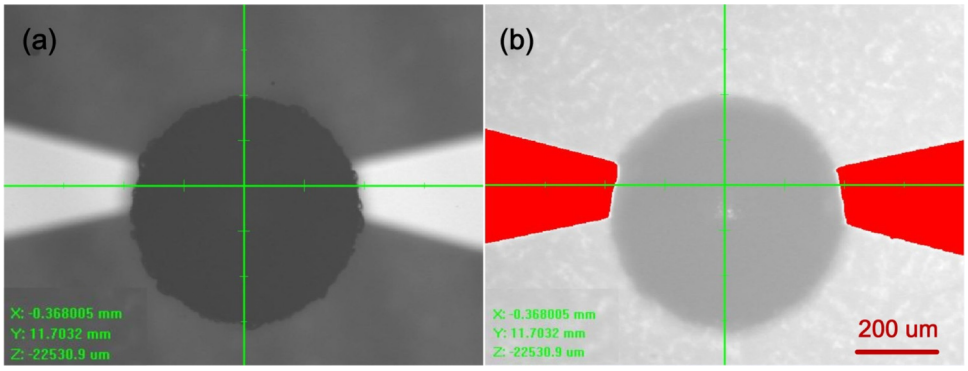

Fig. 4. Images by white light interferometer (WLI) to characterize the depth of the cavity with the interference fringes focused on (a) bottom and (b) top of the cavity.

lower thermal mass contributes to a quick thermal balance of the catalytic sensor, based on calorimetric sensing principle.

The morphology of the alumina with catalyst deposited by screen and inkjet printing is characterized by SEM, as shown in Fig. 8a and b, in which the uniformity and porosity of the patterned sensing materials without any structural crack are verified, and the compatibility between the blasted cone structure and the contact loading method is demonstrated. As shown in Fig. 8c, the catalyst demonstrated good thermal stability after six hours aging treatment.

3.2. Sensing properties

The curves of the sensor response versus methane concentration are shown in Fig. 9, including the blasted sensor and the bulk sensor. Both sensors show linear responses to methane ranging from 0.5% to 2.5%, while the blasted sensor demonstrates higher sensitivity (1.83 mV/% CH_4) than the bulk sensor (1.36 mV/% CH_4) by 35%. This is because more combustion heat is dissipated during the vertical heat transfer procedure from the catalyst to the quartz substrate before thermal balance of the bulk sensor, while the heat transfer in blasted sensor is impeded by the cone-shaped cavity filled by air, with a thermal conductivity of 0.024 W/m · K, much lower than quartz. Meanwhile, the linearity is enhanced with the correlation coefficient, r, of the testing scatters increasing from 0.9856 to 0.9986.

The forward/backward ambient temperature effects on sensors base-line signals are as shown in Fig. 10a and b respectively. With an increased ambient temperature, the thermal loss of the sensor decreases, which increases the working temperature of the sensor and significantly raises the resistance so as to base-line signal of the Pt electrode. However, the influence can be eliminated by utilizing a bridge consists of a sensing/reference pair as differential circuit with temperature coefficient as low as 0.025 mV/°C, which is negligible compared with sensor sensitivity to methane. The sensor shows a slight hysteresis to ambient temperature due to the different dynamic thermal property between sensing and reference elements.

The resistance of the sensors to external mechanical shocks was investigated on the testing platform, as shown in Fig. 11a and b, including the fabricated cone-shaped sensor, and two silicon methane sensors working at their nominal driving voltages at 400–500 °C, and the results are shown in Fig. 11c. The output signal of the silicon membrane sensor (MP7214) shows significant fluctuation influenced by the input typical 50 Hz vibration which is most concerned about in industry field, with the resistance fluctuated by more than 0.3 Ω correspond to a 12 mV bias (nominal current of 40 mA), and thus an equivalent concentration of 1.0% CH_4 (nominal sensitivity of 12 mV/% CH_4), even higher than the alarming valve

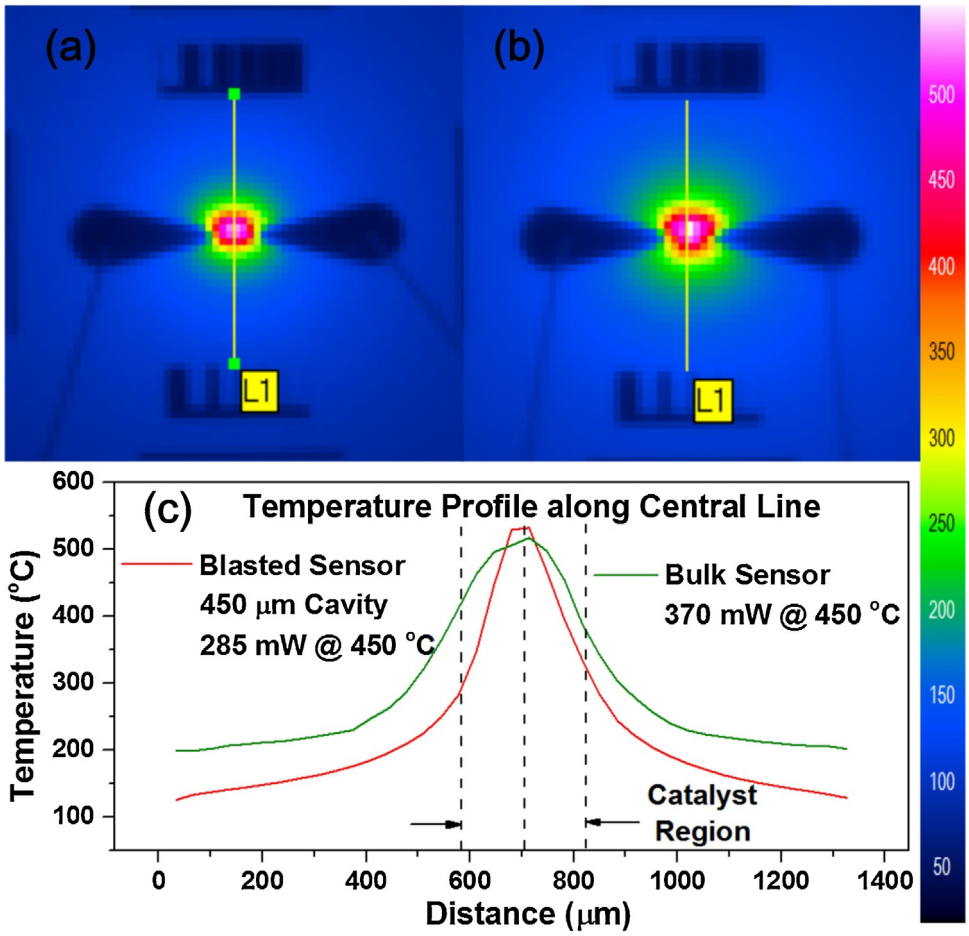

Fig. 5. Thermal characterization results of fabricated devices working at 450 °C by high resolution infrared camera. Comparison of surface temperature distribution profiles between (a) blasted sensor with a 450 μm deep cavity in 500 μm quartz substrate and (b) bulk sensor without a cavity. (c) Comparison of temperature profiles along the central lines (L1) across the surface of alumina support catalyst.

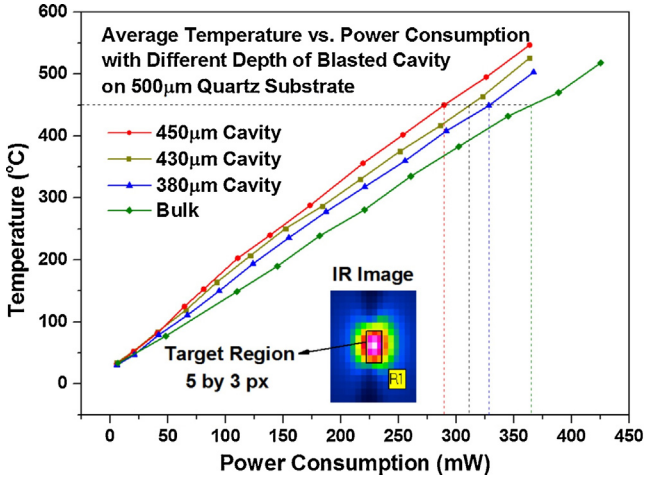

Fig. 6. Curves of average working temperature versus the power consumption of the fabricated sensors with different depth of cavities.

in coal mining. The reason is because the silicon based membrane (normally 1 μm thick Si_3N_4 [19]) and the central loaded catalyst (normally 10 μm thick Pd/Al_2O_3 [21]) form a fixed–fixed beam, sensitive to motions. As a comparison, the fabricated quartz sensor does not need the membrane structure due to its low thermal conductivity, and the cone-shaped structure maintains the strength on both horizontal and vertical directions, demonstrating no obvious sensitivity to inertial motions. Comprehensive resistive properties against swept frequency vibration will be further investigated in future.

4. Conclusion

A quartz MEMS catalytic methane sensor with a back-etched cone cavity was proposed and fabricated by high-resolution abrasive sand blasting, together with lift-off, screen printing and inkjet

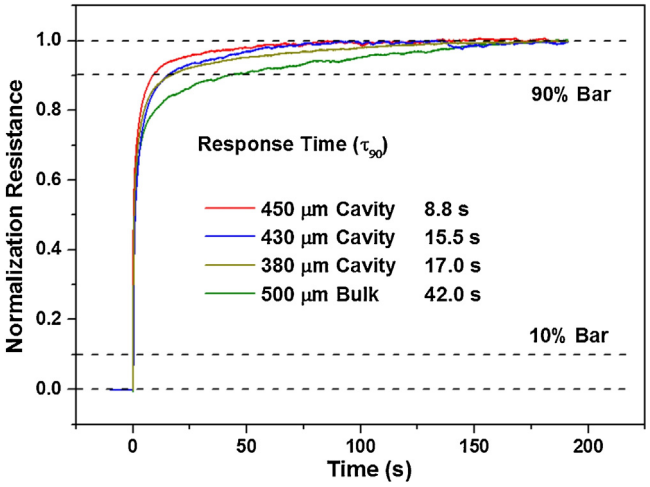

Fig. 7. Waveforms of the sensors' transient resistances responding to the input steps with the same heating power of 280 mW. The thermal response time are characterized by the expended time during the response signal increases from 10% to 90%, and are investigated among the sensors with different depth of cavities.

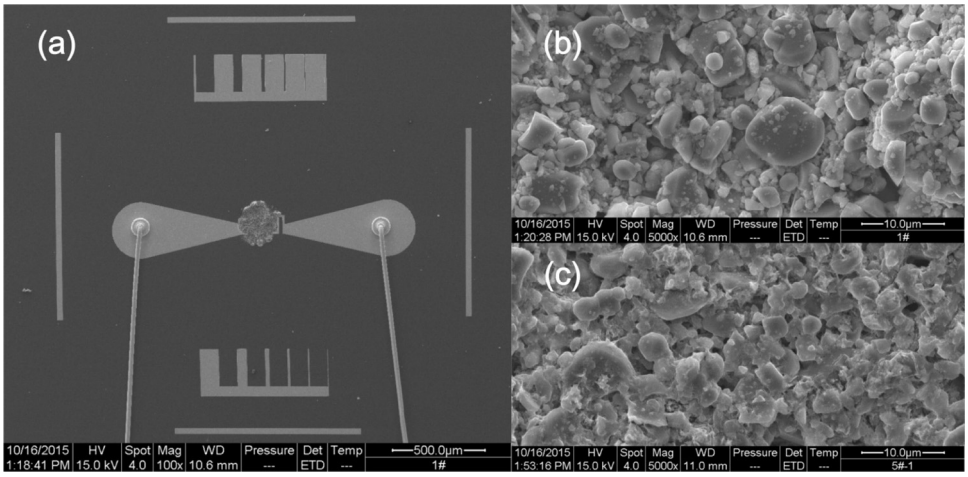

Fig. 8. SEM images of (a) the fabricated sensor with alumina supported bi-metal catalyst deposited on the electrode by screen and inkjet printing, and (b) the porous morphology of the fresh catalytic sensing materials, with alumina particles ranging from 1 to 10 μm, and metal catalyst clusters around hundreds of nanometers. (c) SEM morphology image of catalyst aged in 0.6% methane/air for six hours at working temperature of 450 °C.

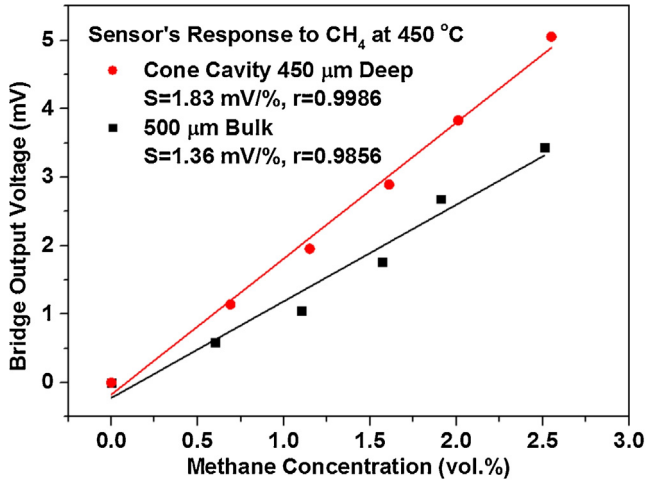

Fig. 9. Sensor's response to methane of concentration from 0.5% to 2.5% balanced by compressed air, with sensitivity (S) and linear correlation coefficient (r) compared between the blasted sensor with a 450 μm deep cavity and the bulk sensor.

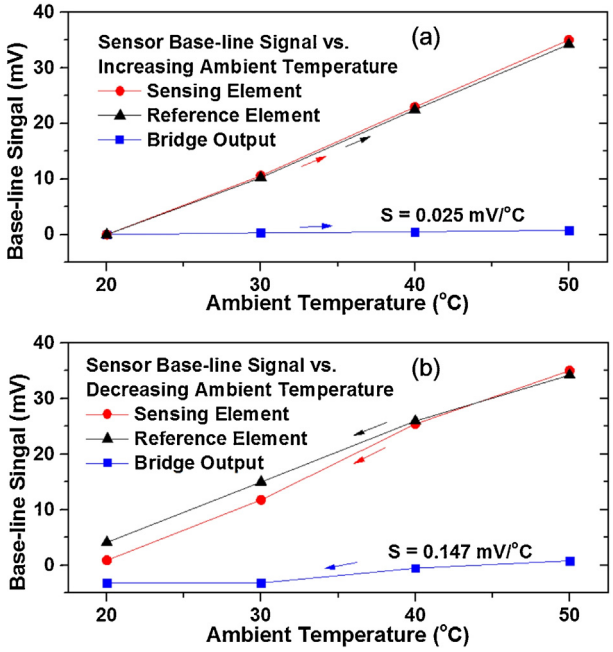

Fig. 10. Sensor base-line signal influenced by (a) increasing and (b) decreasing ambient temperature, including sensing element (with catalyst), reference element (without catalyst), and sensor bridge (differential circuit consists of sensing/reference pair).

printing processes. Uniform cavities 450 μm deep with margin crack less than 10 μm and sidewall roughness less than 1 μm was simply achieved on a fused quartz substrate 500 μm thick with physical etching rate over 380 μm/s. Owing to a lower thermal mass beneath the heating and sensing electrode, the sensor performance was enhanced significantly, verified by FEM simulation and device experiment, with power consumption, response time, and sensitivity optimized to 285 mW, 8.8 s, and 1.83 mV/% CH_4, by 28%, 79%, and 35%, respectively. Compared with conventional silicon based gas sensors, the microfabrication processes of the proposed sensor are highly simplified. Moreover, due to the excellent strength of the cone-shaped structure, the sensor shows good mechanical stability, including the compatibility with contact loading methods of catalyst, and the performance against external shock at high temperature. This simple, fast, but highly uniform fabrication process and reliable performance of the sensor may lead to wide applications to various areas using micro catalytic combustion devices, especially for harsh environmental applications.

Acknowledgement

The authors thank Yanke Peng, Rui You, Yongfeng Gao, Bo Ma, Shuo Chen, and Manxia Hu for assistance in microfabrication. The authors also thank Taipei WaferPlus Co. Ltd., Beijing Capitalbio Co. Ltd., Kunshan SIBCO Co. Ltd., Hong Kong Nikyang Enterprise Ltd., and Engineering Research Center for Navigation Technology at Tsinghua University, for the micro-machining and characterization services.

References

[1] J. Shemshad, S.M. Aminossadati, W.P. Bowen, M.S. Kizil, Effects of pressure and temperature fluctuations on near-infrared measurements of methane in underground coal mines, Appl. Phys. B 106 (2012) 979–986.
[2] A. Kumar, T.M.G. Kingson, R.P. Verma, R. Mandal, S. Dutta, S.K. Chaulya, G.M. Prasad, Application of gas monitoring sensors in underground coal mines and hazardous areas, Int. J. Comput. Technol. Electron. Eng. 3 (2013) 9–23.
[3] Y. Wang, M.M. Tong, D. Zhang, Z. Gao, Improving the performance of catalytic combustion type methane gas sensors using nanostructure elements doped with rare earth cocatalysts, Sensors 11 (2011) 19–31.
[4] Robert W. Howarth, R. Santoro, A. Ingraffea, Methane and the greenhouse-gas footprint of natural gas from shale formations, Clim. Change 106 (2011) 679–690.
[5] M. Cargnello, J.J.D. Jaén, J.C.H. Garrido, K. Bakhmutsky, T. Montini, J.J.C. Gamez, R.J. Gorte, P. Fornasiero, Exceptional activity for methane combustion over modular Pd@CeO_2 subunits on functionalized Al_2O_3, Science 337 (2012) 713–717.
[6] E.E. Karpov, E.F. Karpov, A. Suchkov, S. Mironov, A. Baranov, V. Sleptsov, L. Calliari, Energy efficient planar catalytic sensor for methane measurement, Sens. Actuators A 194 (2013) 176–180.
[7] E. Karpova, S. Mironov, A. Suchkov, A. Karelin, E.E. Karpov, E.F. Karpov, Increase of catalytic sensors stability, Sens. Actuators B 197 (2014) 358–363.
[8] J. Shemshad, S.M. Aminossadati, M.S. Kizil, A review of developments in near infrared methane detection based on tunable diode laser, Sens. Actuators B 171 (172) (2012) 77–92.
[9] L. Boon-Brett, J. Bousek, P. Moretto, Reliability of commercially available hydrogen sensors for detection of hydrogen at critical concentrations: part II—selected sensor test results, Int. J. Hydrogen Energy 34 (2009) 562–571.
[10] Zainab Yunusa, Mohd. Nizar Hamidon, Ahsanul Kaiser, Gas sensors: a review, Sens. Transduc. 168 (2014) 61–75.
[11] J. Chou, Hazardous Gas Monitors, International Sensor Technology, McGraw-Hill Book Company, New York, 2000.

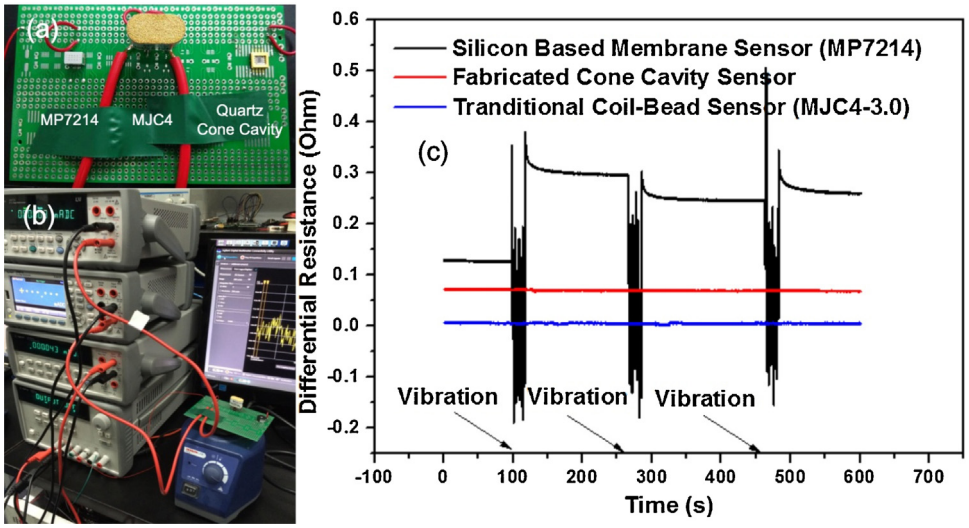

Fig. 11. (a) The mechanical shock testing board integrated commercial silicon based membrane micro pellistor (MP7214), traditional coil-bead sensor (MJC4-3.0), and the fabricated quartz based methane sensor with a cone-shaped cavity and a SOP8 package. (b) The experimental setup for the mechanical test including a vibrator, a set of data acquisition system, and the testing board. (c) Time-domain waveforms of the sensors' output signals responding to external mechanical vibrations.

[12] P.N. Bartlett, S. Guerin, A micromachined calorimetric gas sensor: an application of electrodeposited nanostructured palladium for the detection of combustible gases, Anal. Chem. 75 (2003) 126–132.
[13] A.C. Fischer, F. Forsberg, M. Lapisa, S.J. Bleiker, G. Stemme, N. Roxhed, F. Niklaus, Integrating MEMS and ICs, Microsyst. Nanoeng. 1 (2015) 15005.
[14] A. Mahdavifar, M. Navaei, P.J. Hesketh, M. Findlay, J.R. Stetter, G.W. Hunter, Transient thermal response of micro-thermal conductivity detector (μTCD) for the identification of gas mixtures: an ultra-fast and low power method, Microsyst. Nanoeng. 1 (2015) 15025.
[15] E. Brauns, E. Morsbach, S. Kunz, M. Bäumer, W. Lang, A fast and sensitive catalytic gas sensors for hydrogen detection based on stabilized nanoparticles as catalytic layer, Sens. Actuators B 193 (2014) 895–903.
[16] W. Shin, M. Nishibori, L.F. Houlet, T. Itoh, N. Izu, I. Matsubara, Fabrication of thermoelectric gas sensors on micro-hotplates, Sens. Actuators B 139 (2009) 340–345.
[17] A. Harley, J. Chang, Q. Zhou, J. Dong, T. Pham, M.A. Worsley, R. Maboudian, A. Zettl, W. Mickelson, Catalytic hydrogen sensing using micro heated platinum nanoparticle-loaded graphene aerogel, Sens. Actuators B 206 (2015) 399–406.
[18] L. Xu, Tie Li, X. Gao, Y. Wang, A High Heating Efficiency Two-beam Microhotplate for Catalytic Gas Sensors, NEMS 2012 Kyoto, Japan, March 5–8, 2012.
[19] L. Altmann, H. Sturm, E. Brauns, W. Lang, M. Bäumer, Novel catalytic gas sensors based on functionalized nanoparticle layers, Sens. Actuators B 174 (2012) 145–152.
[20] V. Meille, Review on methods to deposit catalysts on structured surfaces, Appl. Catal. A 315 (2006) 1–17.
[21] L. Xu, Y. Wang, H. Zhou, Y. Wang, Y. Liu, T. Li, Y. Wang, Design, fabrication, and characterization of a high-heating-efficiency 3-D microheater for catalytic gas sensors, J. Microelectromech. Syst. 21 (2012) 1402–1409.
[22] I. Gracia, J. Santander, C. Cane, M.C. Horrillo, I. Sayago, J. Gutierrez, Results on the reliability of silicon macromachined structures for semiconductor gas sensors, Sens. Actuators B 77 (2001) 409–415.
[23] K. Oblov, A. Ivanova, S. Soloviev, N. Samotaev, A. Vasiliev, A. Sokolov, Technology for fast fabrication of glass microhotplates based on the laser processing, Phys. Proc. 72 (2015) 465–469.
[24] D. Briand, S. Colin, A. Gangadharaiah, E. Vela, P. Dubois, L. Thiery, N.F.de Rooij, Micro-hotplates on polyimide for sensors and actuators, Sens. Actuators A 132 (2006) 317–324.
[25] W. Lu, G. Jing, X. Bian, T. Cui, Micro catalytic methane sensor on bulk quartz substrate, in: The 18th International Conference on Solid-State Sensors, Actuators and Microsystems (Transducers 2015), Anchorage, USA, June 21–25, 2015, pp. 1495–1498.
[26] W. Lu, G. Jing, X. Bian, T. Cui, Micro catalytic methane sensor based on inkjet printing technique, in: The 19th International Conference on Miniaturized Systems for Chemistry and Life Sciences (MicroTAS 2015), Gyeonju, Korea,O ctober 25–29, 2015, pp. 1743–1745.
[27] A. Baranov, D. Spirjakin, S. Akbari, A. Somov, Optimization of power consumption for gas sensor nodes: a survey, Sens. Actuators A 233 (2015) 279–289.
[28] J. Spannhake, A. Helwi, A. Friedberger, G. Müller, W. Hellmich, Resistance Heating, Wiley Encyclopedia of Electrical and Electronics Engineering, 1999 http://onlinelibrary.wiley.com/doi/10.1002/047134608X.W3223/full.
[29] Y.J. Min, A.L. Palisoc, C.C. Lee, Transient thermal study of semiconductor devices, IEEE Trans. Compon. Hybrid. Manuf. Technol. 13 (1990) 980–988.
[30] J. Hildenbrand, J. Wöllenstein, E. Spiller, G. Kühner, H. Böttner, G. Urban, J.G. Korvink, Design and fabrication of a novel low cost hotplate micro gas sensor, Design, Test, Integration, and Packaging of MEMS/MOEMS, 2002, Cannes, France, May 6–8, 2002, in: Bernard Courtois, Jean Michel Karam, Karen W. Markus, Bernd Michel, Tamal Mukherjee, James A. Walker (Eds.), Proceedings of SPIE, 4755, 2002.
[31] S. Taze1, B. Cetin, Z. Dursunkaya, Multi-Physics modeling of silicon-Based micro-Grooved heat pip., in: 8th ICCHMT, Istanbul, 25–28 May, 2015.
[32] K. Persson, K. Jansson, S.G. Järås, Characterization and microstructure of Pd and bimetallic Pd–Pt catalysts during methane oxidation, J. Catal. 245 (2007) 401–414.
[33] H. Wang, L. Hou, W. Zhang, A drop-on-demand droplet generator for coating catalytic materials on microhotplates of micropellistor, Sens. Actuators B 183 (2013) 342–349.
[34] W. Lu, G. Jing, X. Bian, H. Yu, T. Cui, A quartz-based micro catalytic methane sensor by high resolution screen printing, J. Micromech. Microeng. 26 (2016) 025021.

Biographies

Wenshuai Lu received the B.S. degree in 2009 and the M.S. degree in 2011, from School of Electrical Engineering and Automation, Harbin Institute of Technology, Harbin, China. He is currently a Ph. D candidate in Department of Precision Instrument at Tsinghua University, Beijing, China. His research interests include MEMS chemical sensors, embedded computing & controlling systems, and The Internet of Things (IoT).

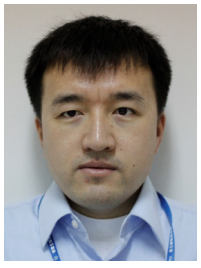

Gaoshan Jing is currently an Associate Professor at Department of Precision Instruments at Tsinghua University, Beijing China. He received his B.S. in Biomedical engineering at Zhejiang University, Hangzhou, China in 1998 and his M.S. in Biophysics at Tsinghua University, Beijing, China in 2001. In 2004, he received his M.S. in Electrical engineering at University of Cincinnati, Cincinnati, Ohio. In 2009, he received his Ph.D. in Electrical Engineering at Lehigh University, Bethlehem, Pennsylvania. His research interests include MEMS/nano sensors for various chemical and biological applications.

Xiaomeng Bian received his B.S. degree from Department of Applied Physics in 2009, at China University of Mining and Technology, Xuzhou, China. In 2013, he got his M.S. Degree of Experimental Condensed Matter Physics at Guangxi Normal University, Guilin, China & Institute of Physics, Chinese Academy of Science, Beijing, China. He is now a Ph.D. student at the Department of Precision Instrument at Tsinghua University, Beijing, China. Currently his research interests include MEMS/NEMS, and new material based electrochemical and catalytic sensors.

Hongyan Yu received the B.S. degree from Department of Software Engineering in 2014, Jiangxi Agricultural University, Nanchang, China. He works at Integrated Microsystems Laboratory in Department of Precision Instrument at Tsinghua University, Beijing, China. His research interests include embedded systems and The Internet of Things (IoT).

Tianhong Cui is currently a Professor of Mechanical Engineering and an Affiliate Senior Member of the graduate faculty in Department of Electrical and Computer Engineering and Department of Biomedical Engineering at the University of Minnesota. He joined the faculty of the University of Minnesota in 2003. From 1995–2003, he held research or faculty positions at Tsinghua University, University of Minnesota, National Laboratory of Metrology in Japan, and Louisiana Tech University, respectively. He was a visiting professor at IMTEK, University of Freiburg in Germany in 2006, and he is holding a visiting professorship at Tsinghua University. His current research interests include MEMS/NEMS and nanotechnology for medical applications.